



Geometric and Dynamic Patterns of the Golmud Segment in the Southern Marginal Fault of the Qaidam Basin

Hao Luo^{1*}, Ji Wang¹, Yasen Gou¹, Hongmei Yu², Peng Shu³ and Zhanwu Gao¹

¹China Earthquake Disaster Prevention Center, China Earthquake Administration, Beijing, China, ²Key Laboratory of Seismic and Volcanic Hazards, Institute of Geology, China Earthquake Administration, Beijing, China, ³Anhui Earthquake Administration, Hefei, China

OPEN ACCESS

Edited by:

Jonny Wu,
University of Houston, United States

Reviewed by:

Feng Cheng,
University of Nevada, Reno,
United States
Xuhua Shi,
Zhejiang University, China

*Correspondence:

Hao Luo
hy-luo@163.com

Specialty section:

This article was submitted to
Structural Geology and Tectonics,
a section of the journal
Frontiers in Earth Science

Received: 01 December 2020

Accepted: 20 May 2021

Published: 01 June 2021

Citation:

Luo H, Wang J, Gou Y, Yu H, Shu P
and Gao Z (2021) Geometric and
Dynamic Patterns of the Golmud
Segment in the Southern Marginal
Fault of the Qaidam Basin.
Front. Earth Sci. 9:636554.
doi: 10.3389/feart.2021.636554

The southern marginal fault of the Qaidam Basin (SMQBF) is a block-bounding border fault that has played a key role in the structural evolution of the Kunlun Fault. However, its geometric and dynamic deformation patterns since the Late Pleistocene have not been clearly observed. Field investigations, combined with high-resolution imagery and shallow seismic profiles, show that the SMQBF is a thrust fault with a sinistral strike-slip component composed of several secondary faults. Its Late Quaternary deformation pattern is characterized by piggyback thrust propagation, and the frontal fault may not be exposed to the surface. Due to the flexural slip of the hanging strata of the secondary fault, sub-parallel faults with widths of thousands of meters have formed on high terraces; these are important when assessing the seismic hazard of this area. Based on high-resolution topographic data obtained using an unmanned aerial vehicle and optically stimulated luminescence chronology, the slip rates of several secondary faults were obtained. The vertical and strike-slip rates of the SMQBF were determined to be 0.96 ± 0.33 mm/a and 2.66 ± 0.50 mm/a, respectively, which may be the minimum rates for the fault. Considering that the SMQBF is composed of several secondary faults, these rates possibly correspond to minimum deformation only. The evident sinistral strike-slip of the SMQBF indicates that although the sinistral slip of the Kunlun Fault system is concentrated in main fault of this system, the branch faults have a significant influence on the lateral extrusion of the Qinghai-Tibet Plateau.

Keywords: flexural slip fault, slip rate, distributed deformation, southern marginal fault of the Qaidam Basin, Kunlun fault

INTRODUCTION

The Indian Plate collided with the Eurasian Plate at 55 ± 5 Ma and has since been continuously moving northward (Dupont-Nivet et al., 2010; Hu et al., 2015). This movement has driven the uplift of the Qinghai-Tibet Plateau and resulted in six large strike-slip faults that border or crosscut the plateau (Tapponnier et al., 2001). Southwest-northeast compression formed the topographic relief of the Kunlun Mountains 30 Ma ago (Mock et al., 1999; Jolivet et al., 2001; Clark et al., 2010; Duvall, et al., 2013; Cheng et al., 2014). An extensional basin began forming in the western segment of the Kunlun Fault before 15 Ma, possibly coincident with volcanic activity (Jolivet et al., 2001), indicating the initiation of a large-scale, sinistral strike-slip displacement of the fault. Duvall et al. (2013) indicated that the strike-slip motion of the Kunlun fault was initiated 20–15 Ma ago. The semi-positive flower structure of the Kunlun Fault is formed by the oblique extrusion of the Qinghai-Tibet Plateau along the Altyn Tagh Fault (Tapponnier et al., 2001; Luo et al., 2013). The southern marginal fault of the Qaidam Basin (SMQBF), which is a northern secondary

fault of the Kunlun flower structure, marks the border of the plateau and the Qaidam Basin (Tang et al., 2002). Seismic-reflection profiles of this area show that the reverse fault, which dips southwestward at an angle of $\sim 45^\circ$, is one of the main structures controlling the northeastward growth of the Kunlun Mountains (Burchfiel et al., 1989; Wang et al., 2011; Cheng et al., 2014; Wu et al., 2014).

Over the last 30 years, considerable effort has been dedicated studying faults with high slip rates (Xu et al., 2005; Cowgill, 2007; Zhang et al., 2007; Cowgill et al., 2009; Elliott et al., 2011; Luo et al., 2019; Cheng et al., 2015a). Several studies have been focused on the Kunlun Fault system. Historical earthquakes and geomorphic features reveal that the Kunlun and Kunlun Mountain Pass Faults have been heavily deformed by multiple earthquakes. Many researchers have focused on the slip rates of the Kunlun Fault which maintains uniform slip-rate (Van der Woerd et al., 2000; Van der Woerd et al., 2002). The 2001 Mw 7.8 earthquake in the Kunlun Mountain Pass Fault further increased the interest in this area (Xu et al., 2005; Klinger et al., 2006; Xu et al., 2006). However, faults with low slip rates have been overlooked. For example, the Longmenshan Thrust Zone was assigned a moderate to low seismic hazard rating before the 2008 Wenchuan Mw 7.9 earthquake, due to the low seismic activity and slow deformation in this area (Xu et al., 2009; Zhang, 2013). The Chelungpu Fault was also not considered seismically active prior to the 1999 Chichi earthquake (Chen et al., 2002), and the fault trace was simply represented by a dashed line on geologic maps (Chang, 1971; Chinese Petroleum Corporation, 1982a, Chinese Petroleum Corporation, 1982b). Nevertheless, faults with long recurrence intervals and minor interseismic deformation could be as destructive as fault with high deformation rates (Zhang, 2013).

The southern marginal fault of the Qaidam Basin (SMQBF) has also experienced earthquakes with very slow deformation rates and had been assigned a low seismic hazard rating (China earthquake administration, 2015). Over the past decades, a few studies have been conducted on the SMQBF, which have reported that it is a large blind fault where the last seismic activity occurred in the Late Pleistocene (Zhou et al., 2009). Because the traces of the SMQBF are indistinguishable due to intense erosion, the activity and faulting behavior of the SMQBF is still not entirely clear. However, this fault is crucial for assessing the regional seismic hazard.

In this study, we present a detailed deformation record of the Late Quaternary fluvial terraces at three sites in the Golmud segment of the SMQBF. Optically stimulated luminescence (OSL) dating was used to constrain the timing of terrace formation and unmanned aerial vehicle (UAV) photogrammetry was utilized to generate a digital elevation model (DEM) for accurate determination of fault offsets. The slip rate and deformation model of the fault since the Late Pleistocene were determined to facilitate seismic hazard assessment of the southern Qaidam Basin and Golmud City, which constitute an important transportation junction of the Qinghai–Tibet Railway in western Qinghai Province.

GEOLOGICAL BACKGROUND

The Qaidam Basin is bordered by the SMQBF, the northern marginal fault of the Qaidam Basin (NMQBF), and the Altyn

Tagh fault to the south, northeast and northwest, respectively (Figure 1). The NMQBF separates the Qaidam Basin and Qilian Mountain, extending ~ 700 km in the E-W direction, and is divided into four sections. The Xitie Mountain and Amoniki Mountain sections offset the youngest alluvial fans, with abandonment ages of 8.9 ± 0.7 ka (Ye et al., 1996), thus, these represent active Holocene faults. Seismic profile interpretations have revealed that the shortening rate of the fault has been approximately 0.73 mm/a since 3.58 Ma (Yuan, 2003).

The middle segment of the Altyn Tagh Fault, located west of the Qaidam Basin, experienced a large-scale sinistral displacement 15 Ma ago (Wu et al., 2012a, Wu et al., 2012b, Wu et al., 2013; Cheng et al., 2015b, Cheng et al., 2016). Its slip rate since the Late Pleistocene, as reported in previous studies, is ~ 10 mm/a (Chen et al., 2013; Cowgill, 2007, Cowgill et al., 2009; Zhang et al., 2007; Gold et al., 2009, 2011), which is consistent with the value of 10 ± 2 mm/a obtained from the Global Positioning System (Bendick et al., 2000; Wallace et al., 2004; He et al., 2013).

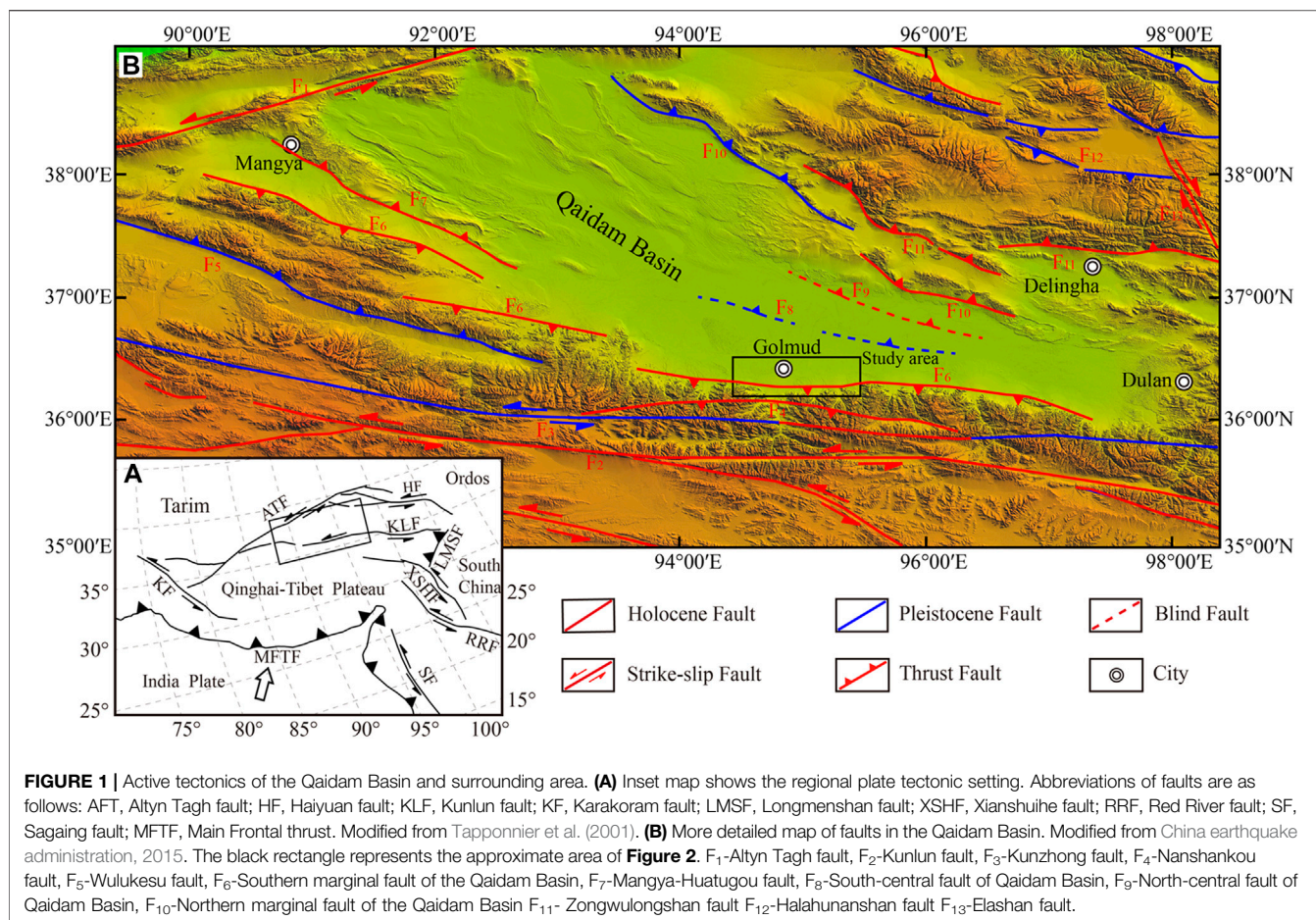
The SMQBF represents the southern boundary of the Qaidam Basin, with an estimated onset age in the Early Paleogene (Zhou et al., 2009). There is no evident continuous linear trace of this fault on the surface (Zhou et al., 2009; Chen et al., 2012). However, the elevation differences between the Kunlun Mountain and Qaidam Basin can reach 2,000–2,500 m. This fault thrusts Proterozoic metamorphic rocks and Late Paleozoic and Mesozoic granites over Cenozoic strata in the basin. The affected strata lie 7–8 km below the surface on the north side of the fault and form the basement of the basin.

The SMQBF underwent intense movement in the Early and Middle Quaternary (Engineering Seismology Research Center, China, 2001). It developed a curved anticline with an axial direction that is consistent with the fault strike in Nuomuhong. North of Xiangride, the fault displaced Early and Middle Pleistocene strata, and the thickness of the Quaternary strata on two sides differ by approximately 600–800 m (Engineering Seismology Research Center, China, 2001). In the Late Quaternary, particularly in the Holocene, the activity of the fault became very weak, and the latest fault activity affected only the Holocene strata within the Utumeiren segment, with five to six magnitude earthquakes (Institute of Crustal Dynamics, China Earthquake, 1992). Secondary faults cutting moraine deposits in the Late–Middle Pleistocene can be observed in some sections near the Golmud segment (Qinghai Petroleum Administration, 1986). Based on seismic profiles, the fault not only displaced the bedrock but also strata from the Paleocene to the Middle Pleistocene, with a dip angle of 45° (Qinghai Petroleum Administration, 1986).

MATERIALS AND METHODS

Surveying the Golmud Segment of the Southern Marginal Fault of the Qaidam Basin

Detailed fault traces of the Golmud segment of SMQBF were mapped using Google Earth imagery to identify topographic



lineaments, fault scarps and offset terraces. We constructed three high-resolution digital elevation models (DEM) using Agisoft Photoscan, based on the structure-from-motion method. At each site, the photographs were captured using a DJI Phantom 4 Pro drone, which is an unmanned aerial vehicle (UAV). The resultant DEMs had a resolution of 3–5 cm/pixel.

Optically Stimulated Luminescence Dating

To constrain the timing of past fault activity, we collected OSL samples on the deformed terraces using stainless steel tube. Each OSL sample was processed under subdued red light, as per the methods of Aitken and Smith (1988) and Lu et al. (2007). Sediments were processed with H₂O₂ and HCl to eliminate organic materials and carbonates. Quartz-rich fractions with diameters of 4–11 μm were etched with 40% HF acid to remove feldspar minerals and alpha-irradiated surfaces of quartz grains. The quartz purity was checked by measuring the infrared stimulated luminescence signal. The etched samples were mounted on stainless steel discs for equivalent dose measurements in accordance with the single-aliquot regenerative dose (SAR) protocols (Murray and Wintle, 2000; Lu et al., 2007). The OSL dating results are listed in **Table 1**.

Slip Rate Calculations

Numerous studies have discussed methods for combining the age and measurements of offset terraces and alluvial fans to determine fault slip rates (Van Der Woerd et al., 2002; Cowgill, 2007; Zhang et al., 2007; Hetzel et al., 2019). We used the riser crest to determine horizontal displacement and upper terrace approach to obtain the age of offset riser (Cowgill, 2007). When projecting the offset riser, the curved riser segment adjacent to the southern scarp would lower the total offset and thus decrease the slip rate. More northerly trending riser projections led to an increased total offset.

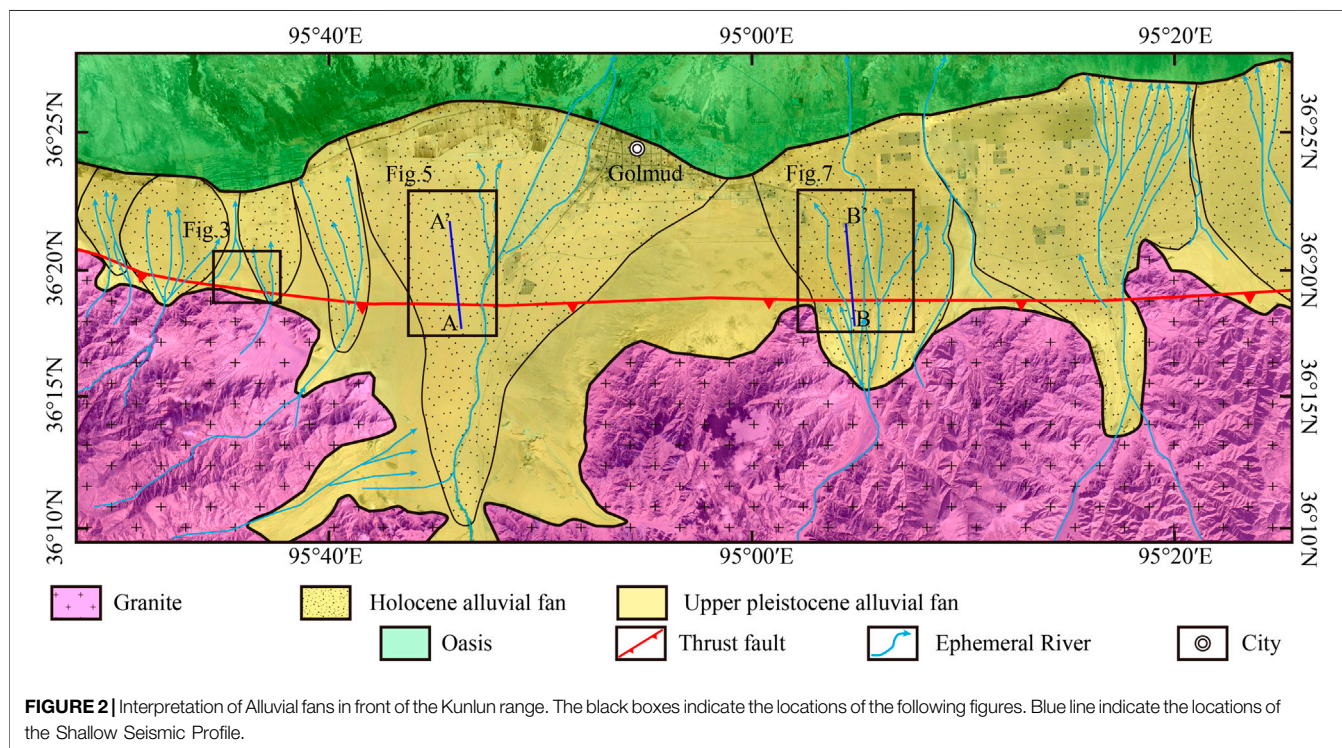
To quantify the vertical fault displacements, we extracted topographic profiles across the fault scarp. Separate straight lines were then fitted to the heights above the scarp and those below the scarp *via* linear regression. The two separate lines were finally projected onto the fault trace to estimate the vertical displacement. We calculated the uncertainties by propagating them in the displacement and terrace abandonment ages.

Shallow Seismic Reflection

To constrain the subsurface structure of the SMQBF, we conducted shallow seismic exploration. For our shallow seismic reflection, we used a multiple time coverage reflection wave method that not only suppresses interference and improves

TABLE 1 | OSL samples and dating results.

Sample Id	Depth (m)	U-238 (Bg/kg)	Th-232 (Bg/kg)	K-40 (Bg/kg)	Water content (%)	Dose rate (Gy/ka)	Equivalent dose (Gy)	Age (ka)
CDMTK-F2-OSL-1	0.6	40.8 ± 4.1	45.6 ± 2.3	490.7 ± 19.6	12.0 ± 5.0	3.37 ± 0.10	69.21 ± 2.98	20.51 ± 2.28
CDMTK-F1-OSL-2	0.6	30.9 ± 1.9	39.9 ± 2.0	466.0 ± 18.6	11.0 ± 5.0	3.10 ± 0.10	38.66 ± 0.69	12.46 ± 1.30
CDMD-T2-OSL-1	0.45	48.8 ± 1.0	46.0 ± 1.8	476.0 ± 19.0	10.1 ± 5.0	3.69 ± 0.10	44.17 ± 1.39	11.97 ± 1.28
GEMD-T1-OSL-1	0.5	30.2 ± 3.3	49.5 ± 4.5	467.9 ± 46.8	9.7 ± 5.0	3.49 ± 0.10	17.85 ± 1.38	5.11 ± 0.66
GEMD-T2-OSL-2	0.5	46.1 ± 0.5	24.5 ± 2.2	496.4 ± 5.0	9.0 ± 5.0	2.96 ± 0.10	29.40 ± 1.71	9.94 ± 1.17



the signal-to-noise ratio of seismic data but also helps determine the existence and form of the fault via a visual image of the subsurface structure. This shallow seismic data acquisition was performed using the ARIES digital seismograph manufactured by CEO-X Corporation. We used a 60 Hz vertical component geophone per receiver station and a 5 m receiver spacing throughout the acquisition of both profiles. Profiles 1 and 2 were acquired with an asymmetric split spread, and were ~5.8 and ~4.08 km in total length, respectively.

RESULT

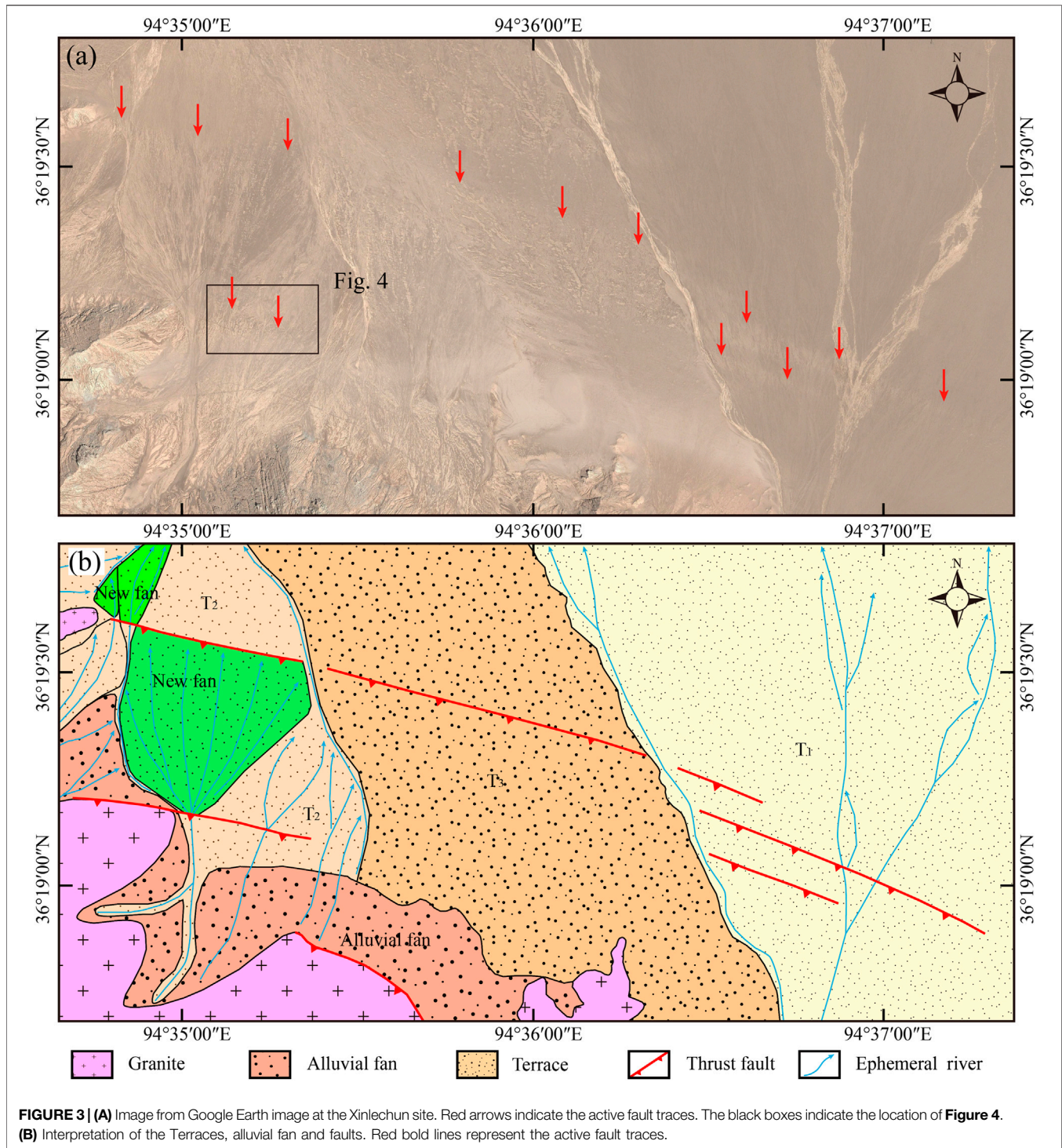
The Golmud segment of the SMQBF does not extend to the surface of the northern alluvial fan in the Kunlun Mountains, although a few gentle deformations and residual scarps can be observed on the terraces. Due to long-term erosion, scarps are

incompletely preserved. Here, we describe the deformations of the alluvial fans at three sites (**Figure 2**). We mapped the deformed Late Pleistocene and Holocene alluvial fan and quantified vertical offsets of several major secondary faults using topographic profiles at the Xinlechun and Hongliugou sites, where the ages of the terraces were determined via OSL dating. We also obtained two shallow seismic profiles at the Golmud and Hongliugou sites.

Terrace Deformation at the Golmud Segment of Southern Marginal Fault of the Qaidam Basin

Terrace Deformation at the Xinlechun Site

The Xinlechun site is located 16 km west of the Golmud River, which forms three different alluvial terraces (**Figure 3**). The third terrace (T_3) is considerably developed, as shown in **Figure 3B**,



while the second terrace (T_2) is developed on the western side of T_3 . There are small seasonal rivers on T_2 , and new alluvial fans have formed due to faulting along the SMQBF. The first terrace (T_1) is developed on the eastern side of T_3 and is the most recent terrace; it was formed by seasonal rivers.

Based on the interpretations of satellite imagery and field investigations, T_1 – T_3 are faulted by the SMQBF. A deformation

zone with a width of ~ 300 m is visible on T_3 . Rows of Middle Pleistocene (Q_2) gravel layers are generally observed on T_3 , and they thrust onto the surface with a 0.5–1 m scarp. Two near-parallel scarps have developed on T_2 , and both have formed new alluvial fans on the northern side of the fault (**Figure 3B**). On T_1 , several rows of approximately parallel surface deformation features were developed in the same deformation zone as that

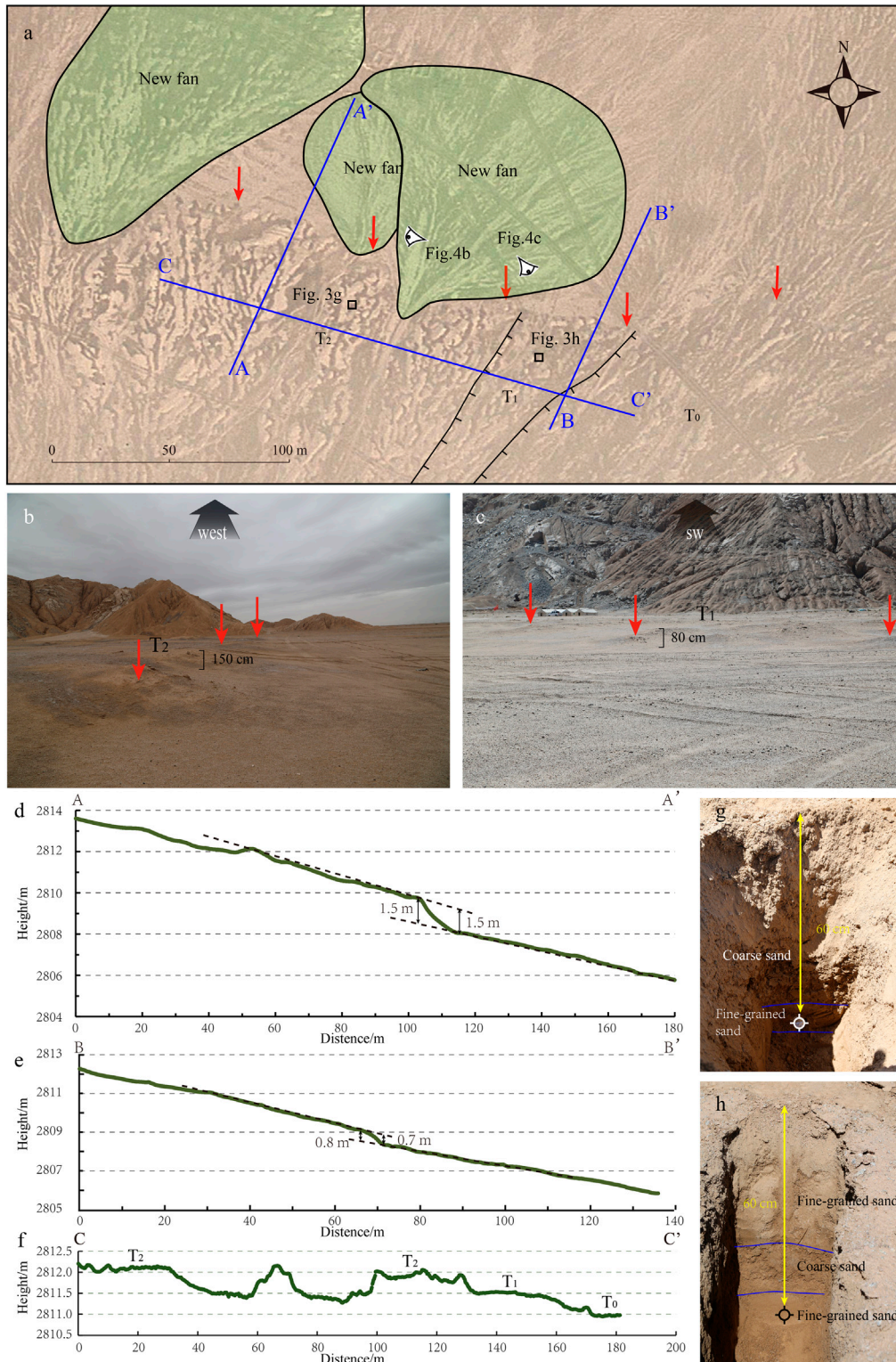
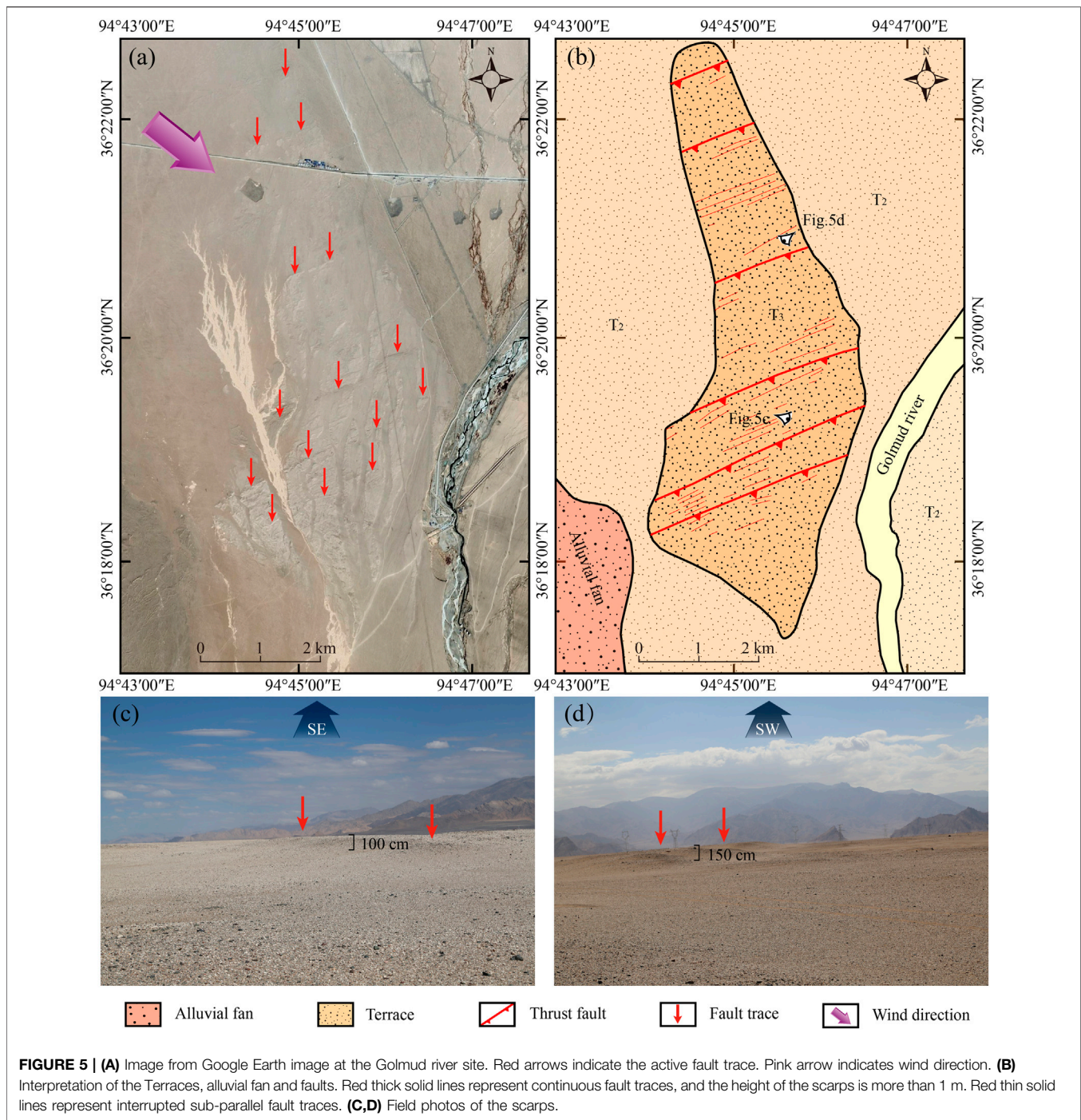


FIGURE 4 | (A) Google Earth image showing active trace of the SMQBF at the Xinlecutn Site. Red arrows indicate conspicuous fault scarps. A-A', B-B' and C-C' represent the location of topographic profiles in **Figures 4D-F**. The small black boxes indicate the location of samples. **(B)** and **(C)** Field photos of the scarps. **(D,E)** Topographic profiles extracted from DEM data used to measure the scarp height. **(F)** Topographic profiles across terrace risers. **(G,H)** OSL sampling photo. Sample site is shown in **Figure 4A**.



of the northern deformation on T_2 ; these features may reflect the youngest deformation zone in this region.

The deformation zone is characterized by gradual pinching outward to the southeast, indicating that deformation has gradually extended toward the southeast. On T_2 , a secondary fault scarp ~500 m in length controls the front of multiple secondary terraces, including T_1 and T_2 . The secondary terraces on the upper wall of the fault have been eroded by seasonal streams, forming new small alluvial fans on the foot wall

(Figure 4A). DEM data on the height of the scarps were used to quantify the vertical displacements of the north-facing fault scarps. A profile across the scarp on T_1 yielded a vertical displacement of 0.75 ± 0.5 m (Figure 4E), whereas another profile across the scarp on T_2 yielded a displacement of 1.5 m (Figure 4D). From this, we inferred that a displacement of 0.75 ± 0.5 m was caused by one paleo-earthquake; thus, the displacement of T_2 may be the product of the accumulation of two paleo-earthquake events.

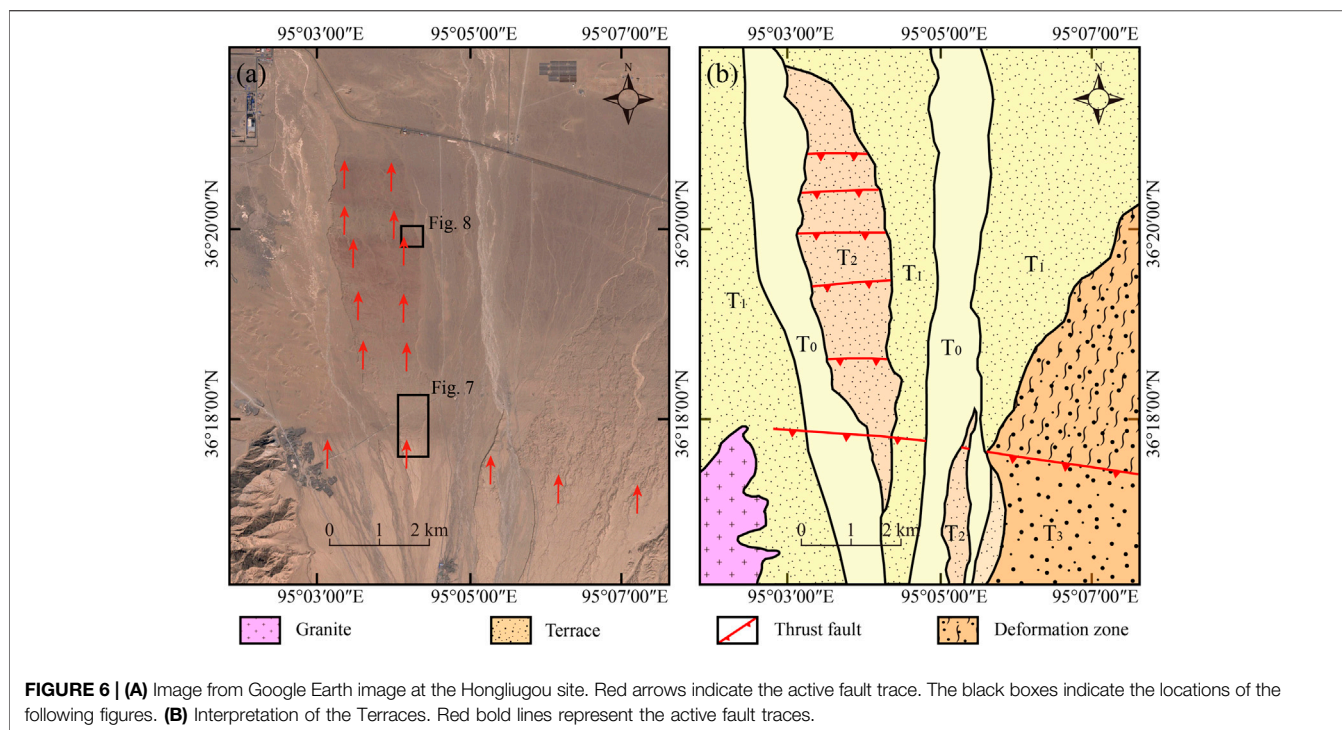


FIGURE 6 | (A) Image from Google Earth image at the Hongliugou site. Red arrows indicate the active fault trace. The black boxes indicate the locations of the following figures. **(B)** Interpretation of the Terraces. Red bold lines represent the active fault traces.

Terrace Deformation at the Golmud River Site

The Golmud River originates from the Kunlun Mountains and flows northward to the Qaidam Basin, forming a large-scale alluvial fan. Three terraces have developed asymmetrically and are preserved with a length of ~10 km from north to south and an approximate width of 4 km from east to west (Figure 5). An OSL dating sample collected from T₃ exhibited an age of 18.89 ± 1.45 ka. Image interpretation and field investigation further revealed that a series of sub-parallel scarps are preserved on T₃ (Figures 5A,B). The scarps may have formed at the same time as the abandonment of T₃ and were subsequently subjected to erosion by braided rivers. The vertical displacements of these scarps are 1.5–2 m (Figures 5C,D).

Numerous small crescent-shaped dunes are deposited on T₂, along the NE320° midcourse direction; this indicates the prevailing wind direction in the study area, which intercepted the scarps at a high angle. Landforms substantially eroded by wind can be seen on T₃. Meanwhile, wind-eroded micro-valleys intersect the parallel scarps and destroy their linear extensions. These features indicate that the parallel scarps were likely formed by tectonic deformation.

Terrace Deformation at the Hongliugou Site

At least three levels of fluvial terraces are developed at the Hongliugou site, east of Golmud, where the terraces were offset by the fault (Figure 6). The deformation width of T₃ is at least 5 km. Due to urban construction, parts of the deformed area have been removed. Braided rivers developed on T₃ and fluvial erosion caused by tectonic deformation led to the fragmentation of the deformed area. During this process, T₃ was severely damaged, although E-W scarps remain identifiable. According to satellite imagery and our field

investigations, T₂, which is located to the east of the seasonal river, has a deformation similar to that of T₃. Due to the weak deformation of T₁, few fault scarps have been found, and we believe that a long interval of seismicity and erosion may have caused the degradation and irregularity of the scarps.

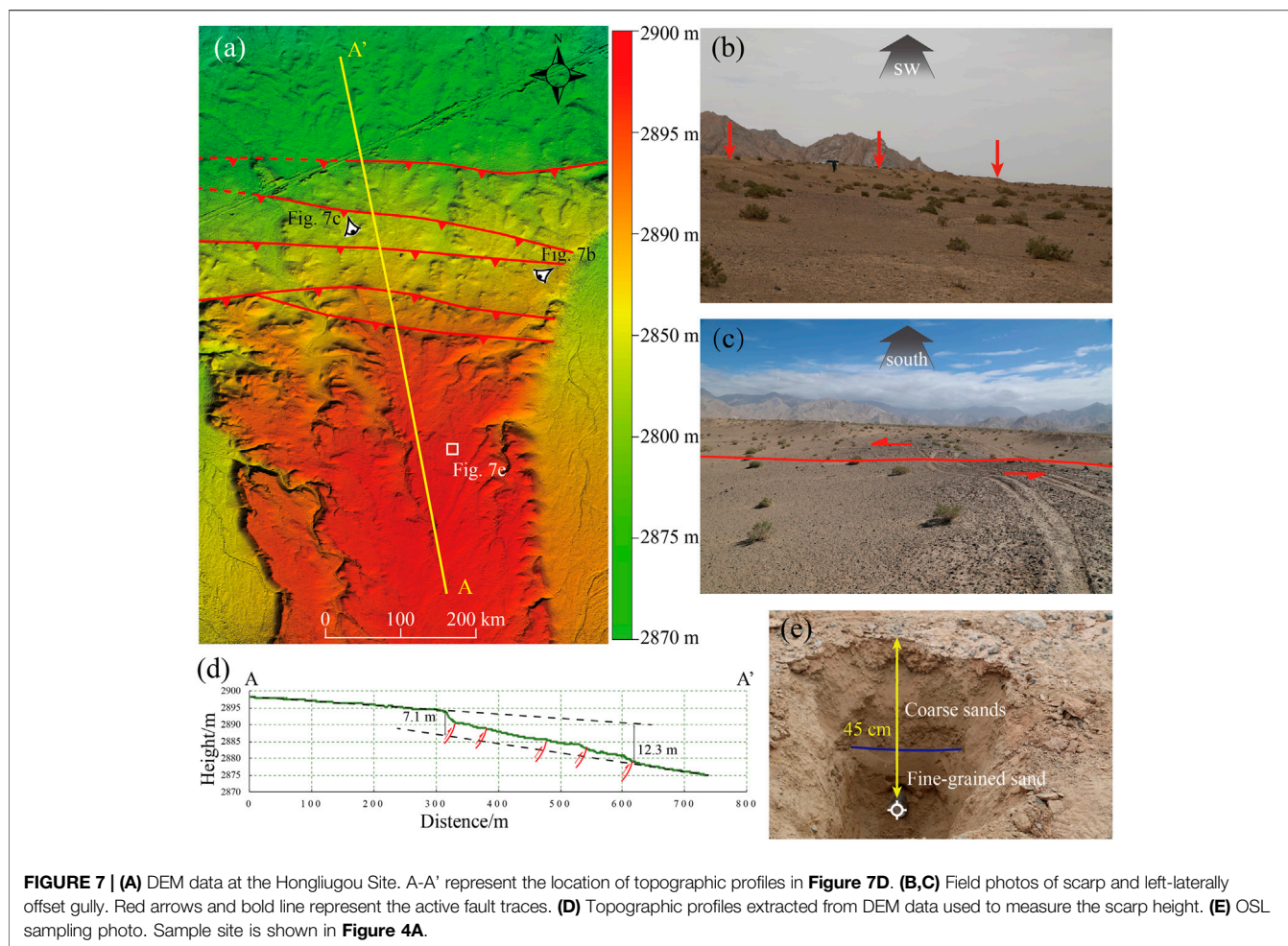
Similar to the Golmud River site, many sub-parallel scarps with E–W orientations formed on T₂. These scarps were likely created by tectonic activities. The southernmost scarps located on T₂ had a deformation width of ~350 m (Figures 7A,B). The scarps were severely eroded, and the deformation zone was composed of several rows of secondary scarps. Some of the residual scarps showed a typical left-lateral strike, with a left-lateral gully displacement of ~3 m (Figure 7C). Image interpretation revealed that the fault caused slight deformation to T₁ and T₀, representing the most recent activity of the sub-fault.

Slip Rate of the Golmud Segment of the Southern Marginal Fault of the Qaidam Basin

Three sites were investigated to estimate the slip rate of the Golmud segment of the SMQBF. The vertical slip rate was investigated at the Xinlecun Site, south Hongliugou Site and north Hongliugou Site, whereas the horizontal slip rate was investigated at the north Hongliugou Site.

Xinlecun Site

We excavated two pits at the tops of two terraces and collected OSL chronology samples. A fine-grained sand lens with a thickness of ~10 cm has developed in T₂' and surrounded by coarse sand 60 cm



below the surface (**Figure 4G**). The sample collected from the lens exhibited an age of 20.51 ± 2.28 ka and was composed of fine sand, which is ideal for OSL dating. We regarded this sample as representative of the age of T_2 . The shallow sediments of T_1 were primarily composed of coarse sand-bearing gravels and fine-grained sands (**Figure 4H**). A sample was collected from a fine-grained sand layer with a thickness of 15 cm, 60 cm below the surface; it exhibited an age of 12.46 ± 1.30 ka.

Considering the OSL derived age of 12.46 ± 1.30 ka from T_2' and a displacement of 0.75 ± 0.05 m, we obtained a vertical slip rate of 0.06 ± 0.01 mm/a. Assuming the age of T_2' to be 20.51 ± 2.28 ka and considering a displacement of 1.5 m, we obtained a vertical slip rate of 0.07 ± 0.01 mm/a. Accordingly, the mean vertical slip rate of the fault was determined to be ~ 0.07 mm/a. Considering that several secondary faults have developed at this site, this rate may be the minimum value for the SMQBF.

South Hongliugou Site

The vertical offsets at the south sub-fault are constrained by topographic profiles perpendicular to the scarp, as shown in the high-resolution DEM. The cumulative vertical offset since the formation of T_2 was estimated to be 9.70 ± 2.60 m (**Figure 7D**). The pit at the top of T_2 showed that the top of the sedimentary

profile, which has a thickness of 30 cm, consists of coarse sands mixed with angular pebbles. The underlying layer has a thickness of 20 cm and comprises fine-grained sand (**Figure 7E**). The OSL sample collected from the bottom of the fine-grained sand showed an age of 11.97 ± 1.28 ka. Based on this age and the 9.70 ± 2.60 m displacement, we obtained a vertical slip rate of 0.85 ± 0.30 mm/a.

North Hongliugou Site

In the front section of the middle deformation region of T_2 , fresh vertical fault scarps suggest that negligible degradation has occurred since the most recent earthquake when compared with the southern scarp (**Figures 8D,E**). Two terraces have developed in this area, and they show a left-lateral strike offset, however, DEM data show that T_1 and T_2 have been left-laterally displaced by 11.00 ± 10 m and 30.50 ± 1.50 m, respectively (**Figure 8A**). To constrain the abandonment age of the two terraces, we hand-dug two pits. The pit from T_1 revealed coarse sands mixed with angular pebbles with a thickness of 20 cm and an underlying layer of fine-grained sand with a thickness of 35 cm, followed by a grayish-green coarse sand layer at the bottom (**Figure 8B**). The OSL sample was collected from the bottom of the fine-grained sand layer

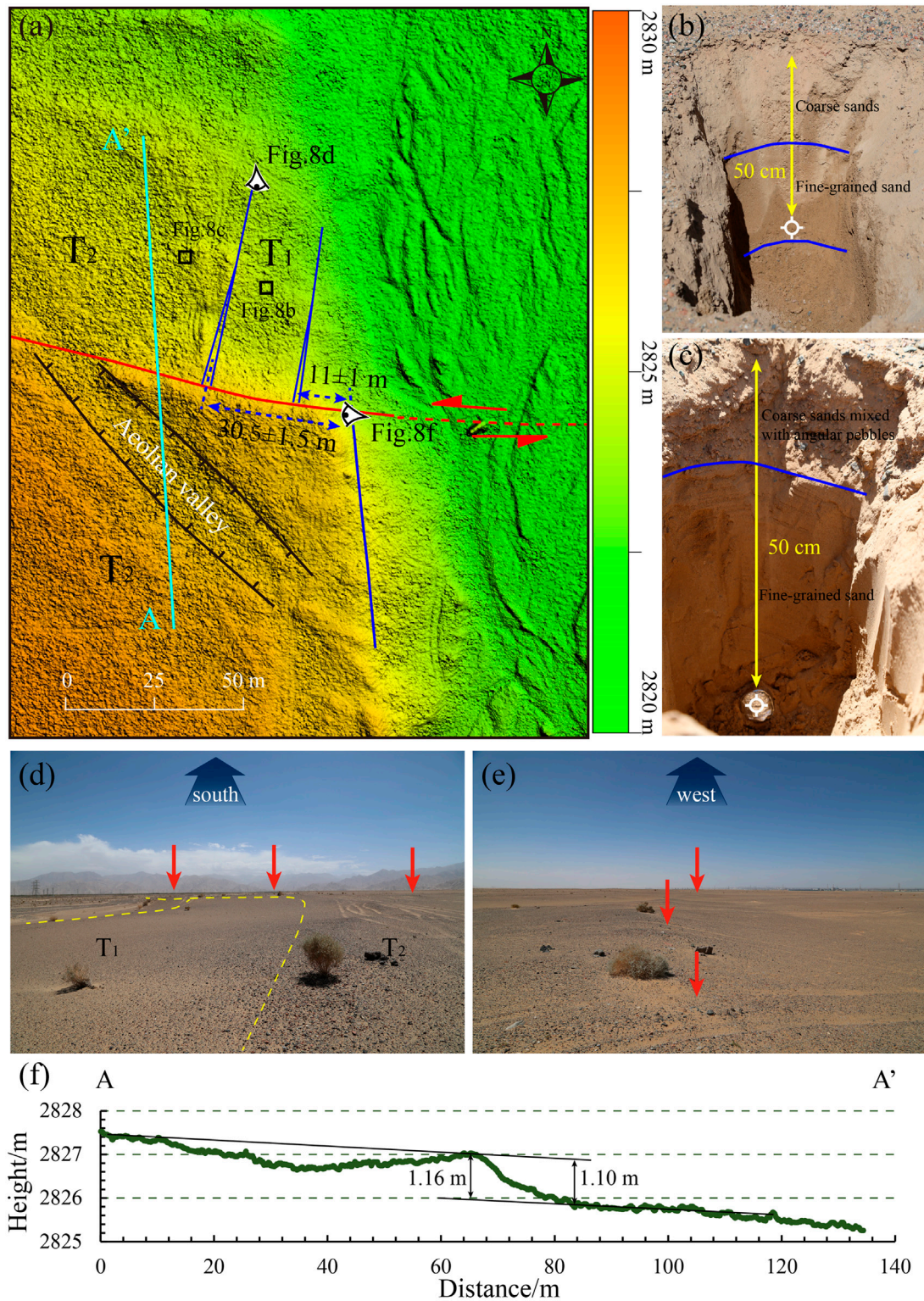


FIGURE 8 | (A) DEM data showing displaced landform at the Hongliugou Site. Red bold line represents the active fault trace, and red dotted line indicates conjectural fault trace. A-A' represent the location of topographic profiles in **Figure 8F**. The small black boxes indicate the location of samples. **(B,C)** OSL sampling photo. Sample site is shown in **Figure 8A**. **(D,E)** Field photos of scarp and left-laterally offset terraces. Red arrows indicate conspicuous fault scarps.

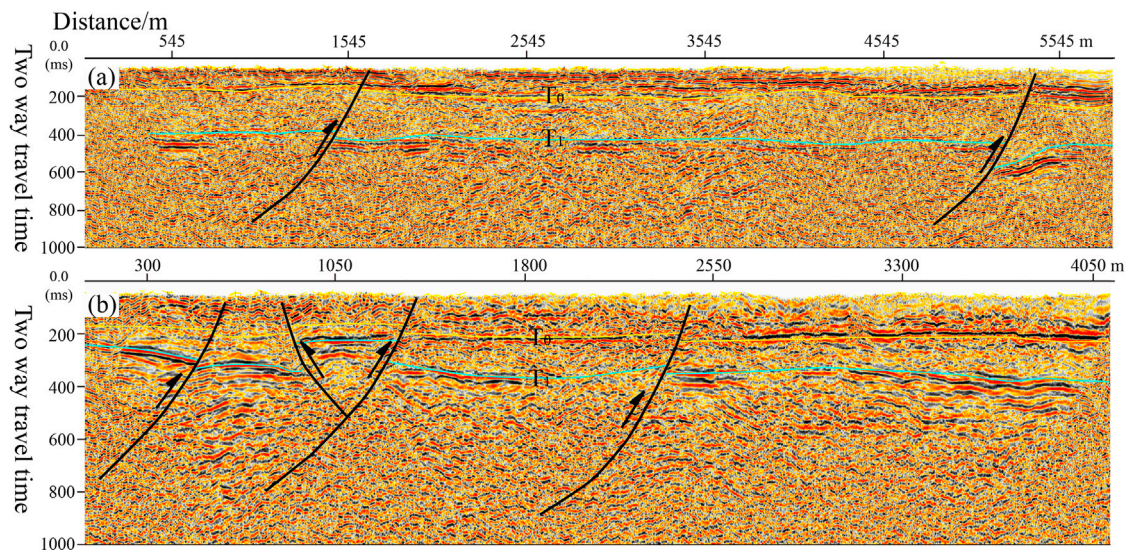


FIGURE 9 | (A) Seismic reflection profiles across SMQBF at Golmud river site is shown in **Figure 2** (Profile A-A'). (B) Seismic reflection profiles across SMQBF at Hongliugou site is shown in **Figure 2** (Profile B-B'). T_0 represents conjectural bottom of the quaternary strata. T_1 represents conjectural bottom of the Cenozoic strata.

50 cm below the surface and exhibited an age of 5.11 ± 0.66 ka. The T_1 pit revealed a 10 cm thick coarse sand layer mixed with angular pebbles; it was underlain by a thickness of 40 cm fine-grained sand layer interbedded with coarse sand, with grayish-green coarse sands at the bottom (**Figure 8C**). The OSL sample was collected from the bottom of the interbedded sand layer 50 cm below the surface, showing an age of 9.94 ± 1.17 ka. Based on the sample age and the displacement of the terraces, we calculated the sinistral strike-slip rates to be 2.20 ± 0.53 mm/a and 3.13 ± 0.48 mm/a for T_1 and T_2 , respectively. The mean sinistral strike-slip rate was found to be 2.66 ± 0.50 mm/a.

The vertical offset of T_2 was estimated to be 1.13 ± 0.03 m (**Figure 8G**). Combining the aforementioned value with the age of T_2 , we obtained a vertical slip rate of 0.12 ± 0.02 mm/a. Therefore, the total vertical slip rate is 0.96 ± 0.33 mm/a at the Hongliugou site, which represents the minimum vertical slip rate of the SMQBF.

Interpretation of the Shallow Seismic Profile

The subsurface structure shown in Profile A-A' reveals two primary faults (**Figure 9A**). The southern secondary fault dips to the south, with an average apparent dip of $\sim 45^\circ$. The northern secondary fault dips to the south, with an average apparent dip of $\sim 50^\circ$. We identified three primary faults in the reflection image of Profile B-B' (**Figure 9B**). The Southern and northern secondary faults are similar to the faults in Profile A-A', and the middle secondary fault forms a back-thrust.

DISCUSSION

Dynamic Rate and Stress Adjustment

The SMQBF has not only absorbed the NE compression of the Qinghai-Tibet Plateau but also shows evident sinistral slip. The

Kunlun and Kunlun Mountain Pass faults are dominantly characterized by sinistral strike-slip, and the slip rate of the middle segment is as high as ~ 12 mm/year (Van Der Woerd et al., 1998; Van Der Woerd et al., 2000; Van Der Woerd et al., 2002). The Kunzhong Fault, which is located between the SMQBF and the Kunlun Fault exhibits evident sinistral strike-slip; a series of gullies are sinistrally displaced by 7–18 m (Wu et al., 1994). Combining age constraints on the offset landforms with the measured sinistral displacement, we determined the left strike-slip rate of the SMQBF to be 2.66 ± 0.50 mm/a. This illustrates that the NE extrusion of the Kunlun Fault is concentrated on the main fault, while the secondary faults also have clear left-lateral strike-slip components.

The variations in slip rates along the Altyn Tagh Fault were quantitatively constrained by the lateral extrusion of the Kunlun Fault system (Luo et al., 2020). The SMQBF is obliquely connected with the Altyn Tagh Fault in the northwest of Mangya city. Tectonic geomorphological studies and Quaternary dating of the offset markers suggest that the slip rate of ~ 10 mm/a along the Altyn Tagh fault is largely consistent on both sides of the inclined zone (Cowgill, 2007; Zhang et al., 2007; Gold et al., 2009; Gold et al., 2011; Gold et al., 2017). This also agrees with the lower shortening and sinistral strike-slip rate of the SMQBF. Due to initiation of sinistral slip along the Kunlun fault 10 Ma ago (Jolivet et al., 2003), the NW-trending mountains within Kunlun mountain system accommodated less sinistral displacement along the Altyn Tagh Fault.

Northward Growth Model of the SMQBF

The kinematics and geometry of the SMQBF were constrained through image interpretation, detailed field studies, and topographic measurements. Offset geomorphological markers suggested that the SMQBF is mainly characterized by a thrust at the Xinlecun site. Two deformation zones were identified, with

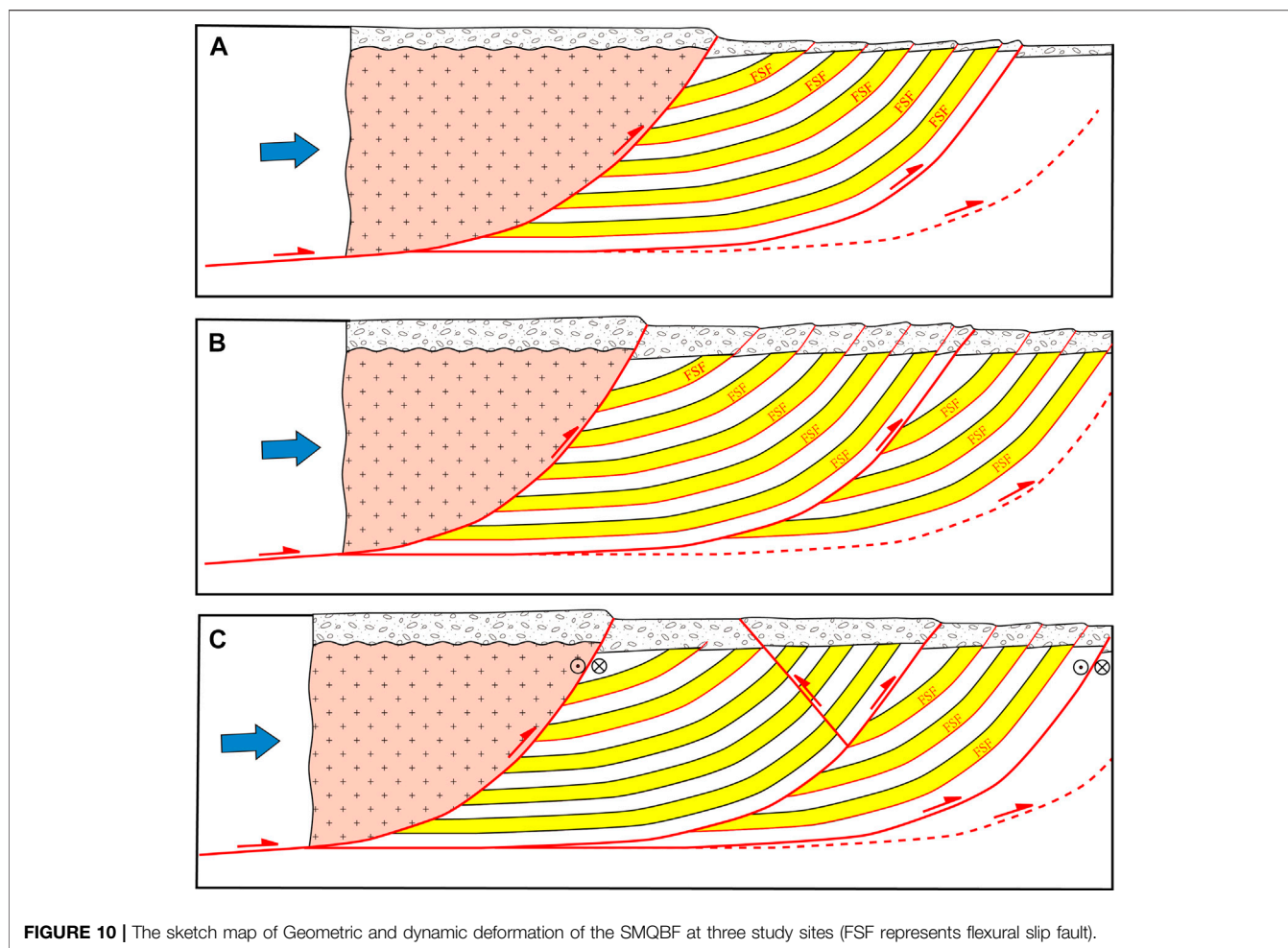


FIGURE 10 | The sketch map of Geometric and dynamic deformation of the SMQBF at three study sites (FSF represents flexural slip fault).

the northern zone showing more recent activity than the southern zone and forming a piggyback thrust propagation sequence from south to north. The offset geomorphology between the two fault deformation zones on T_3 was characterized by several intermittent rows of scarps, which we speculate to have been caused by flexural sliding of the underlying Neogene strata (**Figure 10A**).

A series of sub-parallel scarps was well-preserved at the Golmud River site. The geological profile adjacent to Golmud shows that the SMQBF thrusts into the Paleogene strata up to the Quaternary (Tang et al., 2002). The strata located on the hanging wall of the fault were dominated by Paleogene and Neogene interbedded sandstones and mudstones (Wang et al., 2017), which provided an ideal environment for the formation of flexural faults (Li et al., 2017). The mudstone also played a major role in constraining the structural geometry and surface deformation. Therefore, we infer that the sub-parallel scarps distributed at the Golmud River site were caused by the flexural slip of the hanging wall (**Figure 10B**). While the shallow seismic profile clearly revealed the location of the fault, there are still evident scarps distributed on T_3 on the north of the fault (**Figure 9A**); thus, this fault is likely not the most recent active fault within the SMQBF.

Although the terraces reported herein have been heavily eroded at the Hongliugou site, many sub-parallel scarps are discernible on the southern side of the south scarp. We consider these scarps to have been formed due to the flexural slip of the overlying strata. The shallow seismic profile revealed several sub-faults, one of which forms a back-thrust (**Figure 9B**). We found left-lateral displacements in two deformation zones, indicating the left-lateral strike-slip of the main fault branch. The deformation of T_0 in the southern deformation zone indicates that the surface deformation caused by major earthquakes has not been concentrated in the main fault, as it also occurs on the fault branches and folds of the hanging wall (**Figure 10C**).

Several study sites showed that the SMQBF is characterized by a large deformation width. In this study, the newest deformation zone was not found. Thus, we speculate that the latest activity of the fault may not be exposed at the surface and that a deformation zone >10 km absorbed the north-oriented growth of the Kunlun Fault system.

Significance of Earthquake Disasters

The lower deformation rate of the SMQBF when compared with that of the Kunlun Fault has resulted in under-recognition of the seismic hazard in Golmud. The middle-western segment of the fault, which is 300 km long, has fractured the surface and cut

Quaternary sediments, as evident from satellite imagery. Sub-parallel scarps have formed a ~3 km wide deformation zone in a part of the segment. Due to a lack of field investigations, the slip rate and paleoseismological history have not yet been determined. The earthquake disasters that have previously occurred along the SMQBF are relatively complex and require further study.

Seismic hazards caused by the slow deformation of continental interior regions, where tectonic loading may be shared by an array of faults, are difficult to quantify. Intraplate earthquakes in China are characterized by high magnitudes and millennium-scale recurrence (Ran et al., 2010; Luo et al., 2019), sometimes on the order of 2,000–3,000 years. Therefore, we believe that the seismic recurrence period of the SMQBF, the northern branch of the flower structure of the Kunlun Fault, is relatively long. Because of the high slip rates and occurrence of several major earthquakes along the main Kunlun Fault, we identified a potential seismic hazard for Golmud that has previously been overlooked. The latest branch fault of the SMQBF may extend in front of the alluvial fan and reach Golmud. However, further analyses are needed before a comprehensive earthquake forecast model can be established.

The secondary faults and flexural slip of the SMQBF have formed a wide deformation zone. Although the coseismic displacement of a flexural slip may be small, it can affect the surface and cause damage to or even the collapse of buildings. Golmud City is the starting point of the Qinghai–Tibet engineering corridor, and many pipeline projects pass through the SMQBF. Therefore, a deformation model of the fault established here is critical for city planning in Golmud.

CONCLUSION

The main conclusions from this study are as follows:

- 1) Offset landforms and fault exposures indicate that the SMQBF is a thrust fault with a sinistral strike-slip component characterized by piggyback thrust propagation. A series of sub-parallel scarps formed by flexural slip on the hanging

walls of secondary faults has accommodated the shortening of the SMQBF.

- 2) The vertical and strike-slip rates of the SMQBF were determined to be 0.96 ± 0.33 mm/a and 2.66 ± 0.50 mm/a, respectively, which may be the minimum slip rates for the fault.
- 3) The low deformation rate of the fault may present an under-recognized earthquake hazard. Further investigations should be conducted to assess future seismic hazards in the cities surrounding this fault system.

DATA AVAILABILITY STATEMENT

The original contributions presented in the study are included in the article/Supplementary Material, further inquiries can be directed to the corresponding author.

AUTHOR CONTRIBUTIONS

HL and JW conceived of the study. HL, JW, YG, and ZG carried out field work. PS interpreted shallow seismic profiles. HL and HY wrote the manuscript with input from other authors. All authors contributed to interpretation and discussion of the results.

FUNDING

This work was jointly funded by Spark Program of Earthquake Sciences (XH21047) and Chinese Academy of Sciences, Strategic Priority Research Program (Grant No. XDA20070300).

ACKNOWLEDGMENTS

We would like to thank Editage (www.editage.cn) for English language editing.

REFERENCES

- Aitken, M. J., and Smith, B. W. (1988). Optical Dating: Recuperation after Bleaching. *Quat. Sci. Rev.* 7 (3-4), 387–393. doi:10.1016/0277-3791(88)90034-0
- Bendick, R., Bilham, R., Freymueller, J., Larson, K., and Yin, G. (2000). Geodetic Evidence for a Low Slip Rate in the Altyn Tagh Fault System. *Nature* 404 (6773), 69–72. doi:10.1038/35003555
- Burchfiel, B. C., Quidong, D., Molnar, P., Royden, L., Yipeng, W., Peizhen, Z., et al. (1989). Intracrustal Detachment within Zones of continental Deformation. *Geol* 17 (8), 748–752. doi:10.1130/0091-7613(1989)017<0448:idwzoc>2.3.co;2
- Chang, S. (1971). Subsurface Geologic Study of the Taichuan basin. *Pet. Geology. Taiwan* 8, 21–45. (in Chinese with English abstract)
- Chen, S., Lu, J., Ma, D., Wang, L., Zhao, M., Xue, J., et al. (2012). Origin and Accumulation Characteristics of the Oil from Hanging walls of Kumbel Fault-Terrace belt in Qaidam basin. *Acta Petrolei Sinica* 33 (6), 965–924. (in Chinese with English abstract)
- Chen, Y.-G., Chen, W.-S., Wang, Y., Lo, P.-W., Liu, T.-K., and Lee, J.-C. (2002). Geomorphic Evidence for Prior Earthquakes: Lessons from the 1999 Chichi Earthquake in central Taiwan. *Geol* 30, 171–174. doi:10.1130/0091-7613(2002)030<0171:GEFPEL>2.010.1130/0091-7613(2002)030<0171:gefpel>2.0.co;2
- Chen, Y., Li, S.-H., Sun, J., and Fu, B. (2013). Osl Dating of Offset Streams across the Altyn Tagh Fault: Channel Deflection, Loess Deposition and Implication for the Slip Rate. *Tectonophysics* 594(3), 182–194. doi:10.1016/j.tecto.2013.04.002
- Cheng, F., Guo, Z., Jenkins, H. S., Fu, S., and Cheng, X. (2015b). Initial Rupture and Displacement on the Altyn Tagh Fault, Northern Tibetan Plateau: Constraints Based on Residual Mesozoic to Cenozoic Strata in the Western Qaidam Basin. *Geosphere* 11, 921–942. doi:10.1130/ges01070.1
- Cheng, F., Jolivet, M., Dupont-Nivet, G., Wang, L., Yu, X., and Guo, Z. (2015a). Lateral Extrusion along the Altyn Tagh Fault, Qilian Shan (NE Tibet): Insight from a 3D Crustal Budget. *Terra Nova* 27 (6), 416–425. doi:10.1111/ter.12173
- Cheng, F., Jolivet, M., Fu, S., Zhang, C., Zhang, Q., and Guo, Z. (2016). Large-scale Displacement along the Altyn Tagh Fault (North Tibet) since its Eocene Initiation: Insight from Detrital Zircon U-Pb Geochronology and Subsurface Data. *Tectonophysics* 677-678, 261–279. doi:10.1016/j.tecto.2016.04.023

- Cheng, F., Jolivet, M., Fu, S., Zhang, Q., Guan, S., Yu, X., et al. (2014). Northward Growth of the Qimen Tagh Range: A New Model Accounting for the Late Neogene Strike-Slip Deformation of the SW Qaidam Basin. *Tectonophysics* 632, 32–47. doi:10.1016/j.tecto.2014.05.034
- China Earthquake Administration (2015). *Seismic Ground Motion Parameters Zonation Map of China (GB 18306-2015)* (5th Edn.). Beijing, China: Standards Press of China.
- Chinese Petroleum Corporation (1982b). The Geological Map of Chiayi: Taiwan. *Taiwan Pet. Exploration Division: scale 1, 100000*.
- Chinese Petroleum Corporation (1982a). The Geological Map of Taichung: Taiwan. *Taiwan Pet. Exploration Division: scale 1, 100000*.
- Clark, M. K., Farley, K. A., Zheng, D., Wang, Z., and Duvall, A. R. (2010). Early Cenozoic Faulting of the Northern Tibetan Plateau Margin from Apatite (U-Th)/He Ages. *Earth Planet. Sci. Lett.*, 296(1-2), 78–88. doi:10.1016/j.epsl.2010.04.051
- Cowgill, E., Gold, R. D., Xuanhua, C., Xiao-Feng, W., Arrowsmith, J. R., and Southon, J. (2009). Low Quaternary Slip Rate Reconciles Geodetic and Geologic Rates along the Altyn Tagh Fault, Northwestern Tibet. *Geology* 37 (7), 647–650. doi:10.1130/G25623A.1
- Cowgill, E. (2007). Impact of Riser Reconstructions on Estimation of Secular Variation in Rates of Strike-Slip Faulting: Revisiting the Cherchen River Site along the Altyn Tagh Fault, NW China. *Earth Planet. Sci. Lett.*, 254(3-4), 239–255. doi:10.1016/j.epsl.2006.09.015
- Dupont-Nivet, G., Lippert, P. C., Van Hinsbergen, D. J. J., Meijers, M. J. M., and Kapp, P. (2010). Palaeolatitude and Age of the Indo-Asia Collision: Palaeomagnetic Constraints. *Geophys. J. Int.* 182 (3), 1189–1198. doi:10.1111/j.1365-246x.2010.04697.x
- Duvall, A. R., Clark, M. K., Kirby, E., Farley, K. A., Craddock, W. H., Li, C., et al. (2013). Low-temperature Thermochronometry along the Kunlun and Haiyuan Faults, NE Tibetan Plateau: Evidence for Kinematic Change during Late-Stage Orogenesis. *Tectonics* 32, 1190–1211. doi:10.1002/tect.20072
- Elliott, J. R., Parsons, B., Jackson, J. A., Shan, X., Sloan, R. A., and Walker, R. T. (2011). Depth Segmentation of the Seismogenic continental Crust: The 2008 and 2009 Qaidam Earthquakes. *Geophys. Res. Lett.* 38 (6), 122–133. doi:10.1029/2011gl046897
- Engineering Seismology Research Center, China Earthquake Administration (2001). *Active Fault Identification and Seismic Zoning Report of Key Areas along the Qinghai-Tibet Railway*. (Unpublished)
- Gold, R. D., Cowgill, E., Arrowsmith, J. R., Chen, X., Sharp, W. D., Cooper, K. M., et al. (2011). Faulted Terrace Risers Place New Constraints on the Late Quaternary Slip Rate for the central Altyn Tagh Fault, Northwest Tibet. *Geol. Soc. America Bull.*, 123(5-6), 958–978. doi:10.1130/B30207.1
- Gold, R. D., Cowgill, E., Arrowsmith, J. R., and Friedrich, A. M. (2017). Pulsed Strain Release on the Altyn Tagh Fault, Northwest China. *Earth Planet. Sci. Lett.*, 459, 291–300. doi:10.1016/j.epsl.2016.11.024
- Gold, R. D., Cowgill, E., Arrowsmith, J. R., Gosse, J., Chen, X., and Wang, X. F. (2009). Riser Diachrony, Lateral Erosion, and Uncertainty in Rates of Strike-slip Faulting: A Case Study from Tuzidun along the Altyn Tagh Fault, NW China. *J. Geophys. Res.*, 114(B4). doi:10.1029/2008JB005913
- He, J., Vernant, P., Chéry, J., Wang, W., Lu, S., Ku, W., et al. (2013). Nailing Down the Slip Rate of the Altyn Tagh Fault. *Geophys. Res. Lett.* 40 (20), 5382–5386. doi:10.1002/2013GL057497
- Hetzl, R., Hampel, A., Gebbeken, P., Xu, Q., and Gold, R. D. (2019). A Constant Slip Rate for the Western Qilian Shan Frontal Thrust during the Last 200 Ka Consistent with Gps-Derived and Geological Shortening Rates. *Earth Planet. Sci. Lett.* 509, 100–113. doi:10.1016/j.epsl.2018.12.032
- Hu, X., Garzanti, E., Moore, T., and Raffi, I. (2015). Direct Stratigraphic Dating of India-Asia Collision Onset at the Selandian (Middle Paleocene, 59 ± 1 Ma). *Geology* 43 (10), 859–862. doi:10.1130/g36872.1
- Institute of Crustal Dynamics, China Earthquake Administration (1992). *Seismic Geological Survey and Seismic Risk Analysis of Huatugou—Golmud Oil Pipeline in Qinghai Province*. (unpublished)
- Jolivet, M., Brunel, M., Seward, D., Xu, Z., Yang, J., and Malavieille, J. (2003). Neogene Extension and Volcanism in the Kunlun Fault Zone, Northern Tibet: New Constraints on the Age of the Kunlun Fault. *Tectonics* 22 (5), 7–1. doi:10.1029/2002TC001428
- Jolivet, M., Brunel, M., Seward, D., Xu, Z., Yang, J., Roger, F., et al. (2001). Mesozoic and Cenozoic Tectonics of the Northern Edge of the Tibetan Plateau: Fission-Track Constraints. *Tectonophysics* 343 (1-2), 111–134. doi:10.1016/s0040-1951(01)00196-2
- Klinger, Y., Michel, R., and King, G. (2006). Evidence for an Earthquake Barrier Model from Mw~7.8 Kokoxili (Tibet) Earthquake Slip-Distribution. *Earth Planet. Sci. Lett.* 242 (3-4), 354–364. doi:10.1016/j.epsl.2005.12.003
- Li, T., Chen, J., Thompson Jobe, J. A., and Burbank, D. W. (2017). Active Flexural-Slip Faulting: Controls Exerted by Stratigraphy, Geometry, and Fold Kinematics. *J. Geophys. Res. Solid Earth* 122 (10), 8538–8565. doi:10.1002/2017JB013966
- Lu, Y. C., Wang, X. L., and Wintle, A. G. (2007). A New OSL Chronology for Dust Accumulation in the Last 130,000 Yr for the Chinese Loess Plateau. *Quat. Res.* 67 (1), 152–160. doi:10.1016/j.yqres.2006.08.003
- Luo, H., He, W., Yuan, D., and Shao, Y. (2013). The Holocene Activity Evidence of the Yema River-Daxue Mountain Fault in Western Qilian Mountain. *Acta Geologica Sinica - English Edition* 87 (6), 1569–1584. doi:10.1111/1755-6724.12160
- Luo, H., Xu, X., Gao, Z., Liu, X., Yu, H., and Wu, X. (2019). Spatial and Temporal Distribution of Earthquake Ruptures in the Eastern Segment of the Altyn Tagh Fault, China. *J. Asian Earth Sci.* 173, 263–274. doi:10.1016/j.jseas.2019.01.005
- Luo, H., Xu, X., Liu, X., Bai, L., Wang, Q., Li, M., et al. (2020). Structural Deformation Pattern in the East Segment of the Altyn Tagh Fault. *Acta Geologica Sinica* 94, 692–706. (in Chinese with English abstract)
- Mock, C., Arnaud, N. O., and Cantagrel, J.-M. (1999). An Early Unroofing in Northeastern Tibet? Constraints from 40Ar/39Ar Thermochronology on Granitoids from the Eastern Kunlun Range (Qianghai, Nw china). *Earth Planet. Sci. Lett.* 171 (1), 107–122. doi:10.1016/s0012-821x(99)00133-8
- Murray, A. S., and Wintle, A. G. (2000). Luminescence Dating of Quartz Using an Improved Single-Aliquot Regenerative-Dose Protocol. *Radiat. Measurements* 32 (1), 57–73. doi:10.1016/s1350-4487(99)00253-x
- Qinghai Petroleum Administration (1986). *Regional Structural Characteristics of Qaidam Basin-the Comprehensive Interpretation of the Seismic Reflection of Qaidam Basin*. (unpublished)
- Ran, Y., Chen, L., Chen, J., Wang, H., Chen, G., Yin, J., et al. (2010). Paleoseismic Evidence and Repeat Time of Large Earthquakes at Three Sites along the Longmenshan Fault Zone. *Tectonophysics* 491, 141–153. doi:10.1016/j.tecto.2010.01.009
- Tang, L., Jin, Z., Dai, J., Zhang, M., and Zhang, B. (2002). Regional Fault Systems of Qaidam Basin and Adjacent Orogenic Belts. *Earth Science-Journal China Univ. Geosciences* 27 (06), 21–27. (in Chinese with English abstract)
- Tapponnier, P., Xu, Z., Roger, F., Meyer, B., Arnaud, N., Wittlinger, G., et al. (2001). Oblique Stepwise Rise and Growth of the Tibet Plateau. *Science* 294, 1671–1677. doi:10.1126/science.105978
- Van Der Woerd, J., Ryerson, F. J., Tapponnier, P., Gaudemer, Y., Finkel, R., Meriaux, A. S., et al. (1998). Holocene Left-Slip Rate Determined by Cosmogenic Surface Dating on the Xidatan Segment of the Kunlun Fault (Qinghai, China). *Geol* 26, 695–698. doi:10.1130/0091-7613(1998)0262.3.CO10.1130/0091-7613(1998)026<0695:hlsrdb>2.3.co;22
- Van Der Woerd, J., Ryerson, F. J., Tapponnier, P., Meriaux, A.-S., Gaudemer, Y., Meyer, B., et al. (2000). Uniform Slip-Rate along the Kunlun Fault: Implications for Seismic Behaviour and Large-Scale Tectonics. *Geophys. Res. Lett.* 27 (16), 2353–2356. doi:10.1029/1999GL011292
- Van Der Woerd, J., Tapponnier, P., Ryerson, F. J., Meriaux, A.-S., Meyer, B., Gaudemer, Y., et al. (2002). Uniform Postglacial Slip-Rate along the central 600 Km of the Kunlun Fault (Tibet), from 26Al, 10Be, and 14C Dating of Riser Offsets, and Climatic Origin of the Regional Morphology. *Geophys. J. Int.*, 148, 356–388. doi:10.1046/j.1365-246x.2002.01556.x
- Wallace, K., Yin, G., and Bilham, R. (2004). Inescapable Slow Slip on the Altyn Tagh Fault. *Geophys. Res. Lett.* 31 (9), a–n. doi:10.1029/2004GL019724
- Wang, W., Zheng, W., Zhang, P., Li, Q., Kirby, E., Yuan, D., et al. (2017). Expansion of the Tibetan Plateau during the Neogene. *Nat. Commun.* 8 (1), 1–12. doi:10.1038/ncomms15887
- Wang, Y., Zhang, T., Li, S., Zheng, J., Guo, J., and Sun, G. (2011). Cenozoic Tectonic Deformation Characteristics of Western Qaidam Basin Inferred by Seismic Profile. *Glob. Geology* 30 (2), 213–223. (in Chinese with English abstract)
- Wu, L., Gong, Q., and Qin, S. (2013). When Did Cenozoic Left-Slip along the Altyn Tagh Fault Initiate? A Comprehensive Approach. *Acta Petrologica Sinica* 29 (8), 2837–2850. (in Chinese with English abstract)
- Wu, L., Xiao, A., Ma, D., Li, H., Xu, B., Shen, Y., et al. (2014). Cenozoic Fault Systems in Southwest Qaidam Basin, Northeastern Tibetan Plateau: Geometry,

- Temporal Development, and Significance for Hydrocarbon Accumulation. *Bulletin* 98 (6), 1213–1234. doi:10.1306/11131313087
- Wu, L., Xiao, A., Wang, L., Mao, L., Wang, L., Dong, Y., et al. (2012a). EW-trending Uplifts along the Southern Side of the central Segment of the Altyn Tagh Fault, NW China: Insight into the Rising Mechanism of the Altyn Mountain during the Cenozoic. *Sci. China Earth Sci.* 55, 926–939. doi:10.1007/s11430-012-4402-7
- Wu, L., Xiao, A., Yang, S., Wang, L., Mao, L., Wang, L., et al. (2012b). Two-stage Evolution of the Altyn Tagh Fault during the Cenozoic: New Insight from Provenance Analysis of a Geological Section in NW Qaidam basin, NW China. *Terra Nova* 24 (5), 387–395. doi:10.1111/j.1365-3121.2012.01077.x
- Wu, Z., Wang, Y., and Ren, J. (1994). The Active Faults in the central Tibet Plateau. *Res. active fault* 3, 56–73. (in Chinese with English abstract)
- Xu, X., Wang, F., Zheng, R., Chen, W., Ma, W., Yu, G., et al. (2005). Late Quaternary Sinistral Slip Rate along the Altyn Tagh. *Sci. China Ser. D* 48 (3), 384–397. doi:10.1360/02yd0436
- Xu, X., Wen, X., Yu, G., Chen, G., Klinger, Y., Hubbard, J., et al. (2009). Coseismic Reverse- and Oblique-Slip Surface Faulting Generated by the 2008 Mw 7.9 Wenchuan Earthquake, China. *Geology* 37 (6), 515–518. doi:10.1130/G25462A.1
- Xu, X., Yu, G., Klinger, Y., Tapponnier, P., and Van Der Woerd, J. (2006). Reevaluation of Surface Rupture Parameters and Faulting Segmentation of the 2001 Kunlunshan Earthquake (Mw7.8), Northern Tibetan Plateau, China. *J. Geophys. Res.* 111 (B5), a–n. doi:10.1029/2004JB003488
- Ye, J., Shen, J., Wang, Y., and Ren, J. (1996). The Northern Marginal Active Tectonics of Qaidam Basin. *Res. active fault* 5, 172–180.
- Yuan, D. (2003). *Tectonic Deformation Features and Space-Time Evolution in Northeastern Margin of the Qinghai-Tibetan Plateau since the Late Cenozoic Time*. China Earthquake Administration: Institute of Geology, 1–160. (in Chinese with English abstract)
- Zhang, P.-Z., Molnar, P., and Xu, X. (2007). Late Quaternary and Present-Day Rates of Slip along the Altyn Tagh Fault, Northern Margin of the Tibetan Plateau. *Tectonics*, 26(5, a, n). doi:10.1029/2006TC002014
- Zhang, P. Z. (2013). Beware of Slowly Slipping Faults. *Nat. Geosci.* 6 (6), 323–324. doi:10.1038/ngeo118110.1038/ngeo1811
- Zhou, B., Peng, J., and Zhang, J. (2009). Development and Distribution Patterns of Active Fault Zones in Qinghai Province. *J. Eng. Geology.* 17 (5), 612–618. (in Chinese with English abstract)

Conflict of Interest: The authors declare that the research was conducted in the absence of any commercial or financial relationships that could be construed as a potential conflict of interest.

Copyright © 2021 Luo, Wang, Gou, Yu, Shu and Gao. This is an open-access article distributed under the terms of the Creative Commons Attribution License (CC BY). The use, distribution or reproduction in other forums is permitted, provided the original author(s) and the copyright owner(s) are credited and that the original publication in this journal is cited, in accordance with accepted academic practice. No use, distribution or reproduction is permitted which does not comply with these terms.